Revista Mexicana de Astronomía y Astrofísica, **59**, 201–211 (2023)

https://doi.org/10.22201/ia.01851101p.2023.59.02.05

SPECTROSCOPIC & PHOTOMETRIC STUDY OF THE ALGOL-TYPE BINARY V1241 TAURI

R. H. Nelson[1,2,3], K. B. Alton[2], and M. Kendurkar[3]

Received November 21 2022; accepted March 8 2023

ABSTRACT

New radial velocity (RV) data obtained at the Dominion Astrophysical Observatory (DAO) in Victoria, British Columbia along with light curve (LC) data for the Algol-type binary V1241 Tau have been simultaneously analysed with the 2003 version of the Wilson-Devinney code (WD2003). There were two distinct LC datasets: one was from the Transiting Exoplanet Survey Satellite (TESS) and the others (BVI_c) from the (land-based) Desert Blooms Observatory (DBO). The TESS data were considered to have the least photometric uncertainty; consequently, we derived estimates for M_1 (1.91(8) $M_\odot$), M_2 (1.04(4) $M_\odot$), R_1 (1.86(1) $R_\odot$), R_2 (1.73(1) $R_\odot$), q_{WD} (0.54(3)), L_1 (10.7(8) $L_\odot$), and L_2 (1.7(2) $L_\odot$) following simultaneous analysis (RV+LC) with the WD2003 code. Evolutionary modeling revealed that the primary star is somewhat evolved past the zero age main sequence (ZAMS) while the secondary is much evolved past the terminal age main sequence (TAMS).

RESUMEN

Se analizan simultáneamente datos sobre la velocidad radial de la binaria tipo Algol V1241 Tau obtenidos en el Dominion Astrophysical Observatory en Victoria, Columbia Británica junto con datos sobre su curva de luz. Se usa la versión 2003 del código Wilson-Devinney (WD2003). Los datos sobre la curva de luz provienen de TESS y del Desert Blooms Observatory. Consideramos que los datos de TESS tienen la mejor incertidumbre fotométrica y derivamos estimaciones para M_1 (1.91(8) $M_\odot$), M_2 (1.04(4) $M_\odot$), R_1 (1.86(1) $R_\odot$), R_2 (1.73(1) $R_\odot$), q_{WD} (0.54(3)), L_1 (10.7(8) $L_\odot$), y L_2 (1.7(2) $L_\odot$) después del análisis simultáneo (curva de luz y velocidad radial) con el código WD2003. El análisis evolutivo reveló que la estrella primaria ya se ha alejado un poco de la secuencia principal de edad cero, mientras que la secundaria ya se alejó mucho de la secuencia principal terminal.

Key Words: binaries: eclipsing — binaries: spectroscopic — stars: evolution — stars: fundamental parameters — stars: imaging

1. INTRODUCTION

Following the examination of photographic plates, V1241 Tau (AN 201-1907, BD-01 484, HD 21102, and TYC 4709-1181-1) was discovered to be a variable star in the constellation Taurus by Henrietta Leavitt (Pickering 1908). It was similarly observed by Hoffmeister (1934) who identified the system as Algol-type but the period was not disclosed. Jensch (1934) provided a period of 0.823272 d, along with a light curve and nine times of minima (ToM). Interestingly, this same variable located very near the Eridanus/Taurus border was reported by Gaposchkin (1953) but was instead identified as WX Eri. Not until Kazarovets et al. (2006) did the nomenclature for this eclipsing binary finally change to V1241 Tau. Roman (1956) classified the system (also listed as WX Eri) as A7+F6V. Sarma & Abhyankar (1979) analysed new B and V light curves using the rectification method and tentatively classified WX Eri as detached with the F3 primary pulsating like a δ-Scuti variable with two periods of about 0.16 and 0.14 d. Giuricin & Mardirossian (1981) concluded from their own data that this system was unlikely to be a simple main sequence (MS) detached system. Russo & Milano

[1]Mountain Ash Observatory, BC, Canada.
[2]Desert Blooms Observatory, AZ, USA.
[3]Guest investigator, Dominion Astrophysical Observatory, Victoria, BC, Canada.

(1983) were the first to analyze light curves using a Roche-based (physical) model, namely that of Wilson & Devinney (1971). Srivastava & Kandpal (1986) performed their own photometry in the B and V passbands and detected no δ-Scuti type light variations. After plotting eclipse timings from 1930 to 1980, they concluded that the orbital period was constant. Arentoft et al. (2004) analyzed their own light curve data with the Wilson and Devinney code and also found no evidence for oscillations in the data. Furthermore as reported by Yang et al. (2012), this Algol-type system should be removed as an "oscillating EA" star as defined by Mkrtichian et al. (2003). Finally, sparsely sampled monochromatic light curve data from V1241 Tau were also acquired during the All Sky Automated Survey (Pojmanski 2003) between 2001 and 2009.

Although primarily designed to capture very small host star brightness changes during an exoplanet transit, the TESS Mission (Ricker et al. 2015; Caldwell 2020) also provides a wealth of LC data for many variable stars. A pre-selected number of dwarf main-sequence stars for photometric study were initially targeted using effectively two minutes of total exposure time (2 sec $\times$ 60). The TESS CCD detector bandpass ranges between 600-1000 nm and is centered near the Cousins I band (I_c). One such imaging campaign which captured LC data from V1241 Tau started on October 19, 2018 and ran continuously every 2 min through November 13, 2018. Another 120 s cadence imaging campaign followed between October 22, 2020 and November 16, 2020. Raw flux readings were processed by the TESS Science Processing Operations Center (TESS-SPOC) to remove long term trends using so-called co-trending basis vectors (CBVs). These results identified as pre-search data conditioning simple aperture (PDCSAP) flux are usually cleaner data than the SAP flux. A large number (n=102) of minimum light timings were produced (MAVKA: Andrych & Andronov (2019); Andrych et al. (2020)) from both imaging campaigns. These along with 18 more ToM literature values were used to determine whether any secular changes in the orbital period could be detected from the eclipse timing residuals (Table 2) evaluated between 2012 and 2020. TESS results expressed in BJD$-$TDB were converted to JD in UTC according to Eastman et al. (2010).

Yang et al. (2012) presented new photometry in B and V which they analyzed with the WD2003 code. However, a spatial model newly rendered with Binary Maker 3 (Bradstreet 1993) using their parameters (i=79.9° and q=0.545) reveals that the eclipses are only partial. This is problematic since it has been shown (Terrell & Wilson 2005; Terrell 2022) that for overcontact and semi-detached binaries undergoing partial eclipses, the mass ratio is indeterminate. Therefore, a radial velocity study (RV) was required to reliably determine the mass ratio and total mass. Accordingly, the necessary spectra were obtained at the Dominion Astrophysical Observatory (DAO).

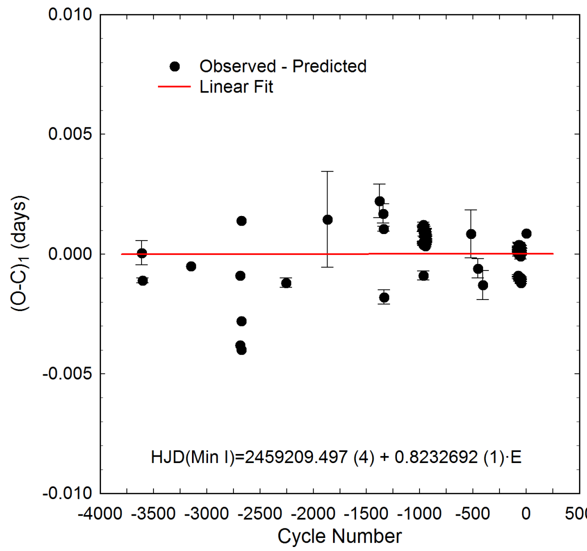

Fig. 1. V1241 Tau: Eclipse Timing Diagram showing straight line fit of O$-$C residuals suggesting no obvious change in the orbital period from 2012 to 2020. The colour figure can be viewed online.

2. PERIOD VARIATION

The first comprehensive period study, using timing data from 1928 to 2011, was by Yang et al. (2012). In it they concluded a linear ephemeris with a light time (LiTE) component due to the orbital movement in conjunction with a supposed third star. Our analysis ignored these data and focused on determining a new linear ephemeris which only included ToM results between 2012 and 2020. This covers the time periods for radial velocity experiments (2014-2015) and the multicolor photometric acquisition of light curve data (2017-2019). These (Table 1) include 18 literature values and 102 ToM estimates extracted from light curve observations made by the TESS Satellite Mission (Ricker et al. 2015; Caldwell 2020) in 2018 and 2020. An eclipse timing difference (O$-$C) plot, is presented in Figure 1. Initially we used the eclipse elements (equation 1) taken from the General Catalogue of Variable Stars (Samus et al. 2017) to seed the linear regression

TABLE 1

V1241 TAU TIMES OF MINIMUM (ToM), MEASUREMENT UNCERTAINTY, EPOCH AND ECLIPSE TIMING DIFFERENCES (ETD) USED TO CALCULATE A LINEAR EPHEMERIS

ToM (HJD-2400000)	Err	Cycle No.	ETD	Ref.	ToM (HJD-2400000)	Err	Cycle No.	ETD	Ref.
56235.4376	0.00050	-3612.5	0.0000	1	58435.6250	0.0001	-940	0.0005	8
56242.4342	0.00010	-3604	-0.0011	1	58436.0367	0.0001	-939.5	0.0006	8
56617.0223	nr	-3149	-0.0005	2	58436.4483	0.0001	-939	0.0006	8
56996.9578	nr	-2687.5	-0.0038	3	58781.8100	0.0010	-519.5	0.0008	9
56996.9607	nr	-2687.5	-0.0009	3	58835.7327	0.0004	-454	-0.0006	9
57006.0135	nr	-2676.5	-0.0040	3	58872.7791	0.0006	-409	-0.0013	10
57006.0147	nr	-2676.5	-0.0028	3	59144.8711	0.0001	-78.5	0.0003	8
57006.0189	nr	-2676.5	0.0014	3	59145.2815	0.0001	-78	-0.0010	8
57351.7894	0.0002	-2256.5	-0.0012	4	59145.6943	0.0001	-77.5	0.0002	8
57672.8670	0.0020	-1866.5	0.0014	5	59146.1048	0.0001	-77	-0.0010	8
58073.7999	0.0007	-1379.5	0.0022	6	59146.5175	0.0001	-76.5	0.0001	8
58101.7905	0.0004	-1345.5	0.0017	6	59146.9281	0.0001	-76	-0.0009	8
58106.3178	0.0001	-1340	0.0010	7	59147.3409	0.0001	-75.5	0.0002	8
58109.6081	0.0003	-1336	-0.0018	6	59147.7513	0.0001	-75	-0.0010	8
58411.3391	0.0001	-969.5	0.0011	8	59148.1643	0.0001	-74.5	0.0004	8
58411.7501	0.0001	-969	0.0005	8	59148.5745	0.0001	-74	-0.0010	8
58412.1623	0.0001	-968.5	0.0010	8	59148.9873	0.0001	-73.5	0.0001	8
58412.5733	0.0001	-968	0.0004	8	59149.3979	0.0001	-73	-0.0010	8
58412.9856	0.0001	-967.5	0.0010	8	59149.8105	0.0001	-72.5	0.0000	8
58413.3967	0.0001	-967	0.0005	8	59150.2211	0.0001	-72	-0.0010	8
58413.8069	0.0001	-966.5	-0.0009	8	59150.6339	0.0001	-71.5	0.0002	8
58414.2200	0.0001	-966	0.0005	8	59151.0444	0.0001	-71	-0.0010	8
58414.6323	0.0001	-965.5	0.0012	8	59151.4571	0.0001	-70.5	0.0001	8
58415.0432	0.0001	-965	0.0005	8	59151.8676	0.0001	-70	-0.0010	8
58415.4555	0.0001	-964.5	0.0011	8	59152.2807	0.0001	-69.5	0.0004	8
58415.8664	0.0001	-964	0.0004	8	59152.6910	0.0001	-69	-0.0010	8
58416.2787	0.0001	-963.5	0.0011	8	59153.1037	0.0001	-68.5	0.0001	8
58416.6897	0.0001	-963	0.0004	8	59153.5142	0.0001	-68	-0.0010	8
58417.1018	0.0001	-962.5	0.0009	8	59153.9272	0.0001	-67.5	0.0004	8
58417.5130	0.0001	-962	0.0005	8	59154.3374	0.0001	-67	-0.0011	8
58417.9253	0.0001	-961.5	0.0011	8	59154.7502	0.0001	-66.5	0.0001	8
58418.3362	0.0001	-961	0.0004	8	59155.1607	0.0001	-66	-0.0011	8
58421.6293	0.0001	-957	0.0004	8	59155.5736	0.0001	-65.5	0.0002	8
58422.0416	0.0001	-956.5	0.0010	8	59159.2770	0.0001	-61	-0.0011	8
58422.4526	0.0001	-956	0.0004	8	59159.6900	0.0001	-60.5	0.0003	8
58424.9224	0.0001	-953	0.0004	8	59160.1003	0.0001	-60	-0.0011	8
58425.3344	0.0001	-952.5	0.0008	8	59160.5133	0.0001	-59.5	0.0003	8
58425.7456	0.0001	-952	0.0004	8	59160.9235	0.0001	-59	-0.0011	8
58426.1576	0.0001	-951.5	0.0008	8	59161.3364	0.0001	-58.5	0.0001	8
58426.5690	0.0001	-951	0.0005	8	59161.7468	0.0001	-58	-0.0011	8
58426.9809	0.0001	-950.5	0.0008	8	59162.1598	0.0001	-57.5	0.0003	8
58427.3923	0.0001	-950	0.0005	8	59162.5701	0.0001	-57	-0.0011	8
58427.8042	0.0001	-949.5	0.0008	8	59162.9829	0.0001	-56.5	0.0001	8
58428.2155	0.0001	-949	0.0004	8	59163.3934	0.0001	-56	-0.0011	8
58428.6273	0.0001	-948.5	0.0007	8	59163.8062	0.0001	-55.5	0.0002	8
58429.0387	0.0001	-948	0.0003	8	59164.2166	0.0001	-55	-0.0011	8
58429.4507	0.0001	-947.5	0.0008	8	59164.6292	0.0001	-54.5	-0.0001	8
58429.8620	0.0001	-947	0.0004	8	59165.0398	0.0001	-54	-0.0011	8
58430.2739	0.0001	-946.5	0.0007	8	59165.4527	0.0001	-53.5	0.0000	8
58430.6854	0.0001	-946	0.0005	8	59165.8632	0.0001	-53	-0.0010	8
58431.0973	0.0001	-945.5	0.0008	8	59166.2761	0.0001	-52.5	0.0002	8
58431.5086	0.0001	-945	0.0005	8	59166.6865	0.0001	-52	-0.0010	8
58431.9207	0.0001	-944.5	0.0009	8	59167.0992	0.0001	-51.5	0.0000	8
58432.3318	0.0001	-944	0.0004	8	59167.5096	0.0001	-51	-0.0011	8
58432.7439	0.0001	-943.5	0.0008	8	59167.9226	0.0001	-50.5	0.0002	8
58433.1551	0.0001	-943	0.0004	8	59168.3328	0.0001	-50	-0.0012	8

a: nr=not reported.

1. Karampotsiou et al. (2016); 2. Nagai (2014); 3. Nagai (2015); 4. Nelson (2016); 5. Nelson (2017); 6. Nelson (2018); 7. Lehký et al. (2021); 8. This study derived from TESS: Ricker et al. (2015); 9. Nelson (2020a); 10. Samolyk (2020); 11. Nagai (2021).

TABLE 1. CONTINUED

ToM (HJD-2400000)	Err	Cycle No.	ETD	Ref.	ToM (HJD-2400000)	Err	Cycle No.	ETD	Ref.
58433.5673	0.0001	-942.5	0.0010	8	59168.7459	0.0001	-49.5	0.0002	8
58433.9785	0.0001	-942	0.0006	8	59169.1563	0.0001	-49	-0.0011	8
58434.3902	0.0001	-941.5	0.0006	8	59169.5691	0.0001	-48.5	0.0001	8
58434.8017	0.0001	-941	0.0005	8	59209.9100	nr	0.5	0.0009	11
58435.2135	0.0001	-940.5	0.0007	8					

a: nr=not reported.
1. Karampotsiou et al. (2016); 2. Nagai (2014); 3. Nagai (2015); 4. Nelson (2016); 5. Nelson (2017); 6. Nelson (2018); 7. Lehký et al. (2021); 8. This study derived from TESS: Ricker et al. (2015); 9. Nelson (2020a); 10. Samolyk (2020); 11. Nagai (2021).

model fit:

$$Min(HJD) = 2\,427\,531.687 + 0.82327038 \cdot E\,, \quad (1)$$

which ultimately led to the following (unweighted) least squares best-fit linear ephemeris used for all phasing:

$$MinI(HJD) = 2\,459\,209.497(6) + 0.8232692(1) \cdot E. \quad (2)$$

3. SPECTROSCOPIC OBSERVATIONS

In September of 2014, and again in September-October of 2015, we obtained a total of 12 medium-resolution (R≈10,000) spectra at the Dominion Astrophysical Observatory (DAO) in Victoria, British Columbia, Canada using the 1.83-m Plaskett telescope. The spectrograph was fitted with a 21181Yb grating (1800 lines/mm and blazed at 5000 Angstroms), producing a reciprocal dispersion of approximately 10 Å/mm. The wavelength range was from 5000 to 5250 Å, and chosen to include the strong iron absorption lines at 5167.487 and 5171.595 Å. Spectra from an iron-argon lamp taken immediately before and after each stellar spectrum were used for wavelength calibration. RV standard stars were selected from the 1986 *Astronomical Almanac* (Section H42-3), many of which were also listed as suitable IAU radial velocity standard stars (Stefanik et al. 1999). These have proven to be extremely reliable and consistent with the results achieved in over 20 publications using the same 1.83-m telescope. In general, stars were selected near in spectral type (and luminosity class) to the target stars (typically A-F, luminosity class V) and as bright as possible. Typical exposures of standards (running from magnitude 2 to 8) on a 1.5-2 metre class telescope run from a few seconds to perhaps 10 or 20 min. Windows software *RaVeRe*, written by the first author and available on his website (Nelson 2013), was used for reduction. The radial velocities were determined by the broadening functions (BF) routine (Ruciński 1969, 1992, 2004) as implemented in the Windows-based software *Broad* (Nelson 2013); details regarding this procedure are provided in Nelson (2010). The elements used for all phasing are given in equation 2. A log of observations and the derived heliocentric radial velocities ($RV_{1,2}$) is presented in Table 2. The calibrated one-dimensional spectra, sorted by phase, are presented in Figure 2. To disentangle the components, Gaussian profile curve fitting was used; see Nelson (2022) for details of the procedure. Figure 3 shows the broadening peaks at phase 0.248 (top) and phase 0.758 (bottom) for the standard and target spectra as indicated in the figure captions.

Derived (heliocentric) RV values are listed in Table 2 along with the uncertainty estimate for each, the latter being the standard deviation of values from the different comparison stars. A double sinusoidal fit to the RV curves yielded the following values: $K_1 = 101.6 \pm 1.8$ km·s^{-1}, $K_2 = 205.5 \pm 4.0$ km·s^{-1}, $V_\gamma = 17.4 \pm 1.8$ km·s^{-1} (systemic velocity), and q_{sp} $(M_2/M_1) = 0.495 \pm 0.012$.

4. PHOTOMETRIC OBSERVATIONS

Photometric observations were carried out at Desert Blooms Observatory (DBO) in 2017 (November, December), 2018 (October) and in 2019 (October, December) during which a total of 1080, 997, and 1081 observations in B, V, and I_c were respectively obtained. The telescope is a 40 cm Schmidt-Cassegrain optical assembly operating at $f/6.8$; data acquisition in 2017 and 2018 was with a SBIG STT-1603; however, in 2019 a QSI 683 CCD camera was used instead (see Nelson 2020b for more details).

In Table 3, J2000 coordinates for the stars of interest are from Gaia EDR3 (Gaia Collaboration 2021) while magnitudes are taken from the AAVSO Photometric All-Sky Survey (APASS DR9; Henden et al. (2009). The colour index $(B{-}V)$ of the comparison was higher than one would like; unfortunately, most candidates in the same field-of-view had similar values. The star chosen for the comparison had the advantage of close proximity on the image

TABLE 2

LOG OF DAO OBSERVATIONS AND RESULTS

DAO Image #	Mid-time HJD-2400000	Exposure (s)	Phase at Mid-exp	RV_1 ($km \cdot s^{-1}$)	RV_2 ($km \cdot s^{-1}$)
15-13226	57297.9750	2400	0.133	-50.5 (3.1)	179.7 (5.6)
15-13235	57298.0082	1804	0.174	-71.5 (3)	201.2 (9.4)
15-13082	57293.9532	1200	0.248	-81.8 (3.4)	217.7 (8.2)
14-24522	56911.9805	1200	0.278	-87.6 (7.0)	214.1 (17.8)
14-24524	56911.9952	1200	0.296	-80.9 (6.9)	214.5 (15.6)
14-24526	56912.0105	1200	0.314	-78.3 (7.0)	203.2 (16.9)
15-13254	57298.9642	2400	0.335	-67.0 (3.4)	193.3 (9.1)
15-13296	57299.9917	2400	0.583	69.8 (4.0)	...
14-24429	56909.0123	836	0.672	98.3 (8.1)	-154.7 (11.1)
14-24432	56909.0364	1200	0.702	114.7 (3.1)	-181.0 (13.2)
15-13018	57291.9030	1200	0.758	126.1 (3.1)	-192.3 (8.7)
15-13182	57296.9164	1800	0.847	104.9 (3.1)	-160.4 (4.8)

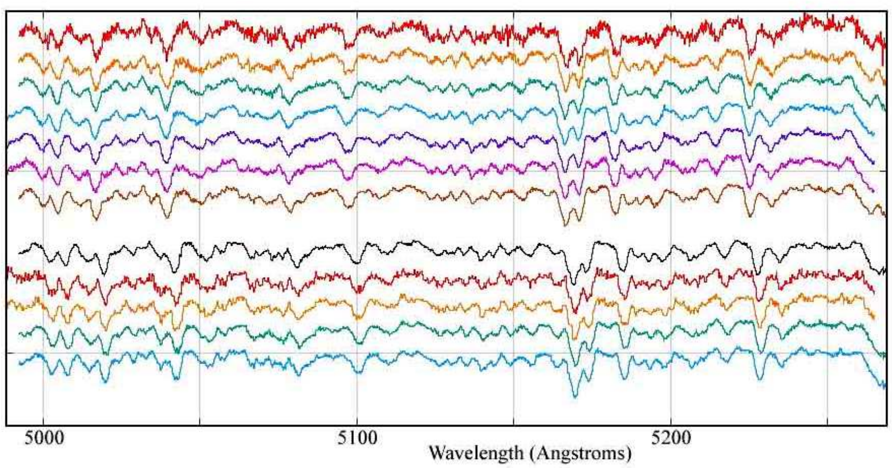

Fig. 2. V1241 Tau spectra, offset for clarity. The vertical scale is arbitrary. The phases (from top to bottom) correspond to those in Table 2, top to bottom. The colour figure can be viewed online.

and being close in brightness to the program star. For all runs, the Comp-Check difference was constant to within ≈0.01 magnitude, with no systematic variation. As described in Nelson (2020b), automatic focusing was required to accommodate the large swings in desert temperature throughout each night. The usual bias, dark subtraction, and flat fielding, as well as aperture photometry was accomplished with MIRA (`https://www.mirametrics.com/`).

5. LIGHT CURVE ANALYSIS

All light curves were normalized relative to maximum flux. RV and light curve data from this paper were simultaneously fit with the WD2003 code which implemented Kurucz atmospheres (Wilson & Devinney 1971; Wilson 1990; Kurucz 1993; Kallrath et al. 1998). This was conveniently packaged as a Windows compatible front-end program with a GUI interface ($WDwint56c$ (Nelson 2013)).

As mentioned earlier, the spectral classification assigned by Roman (1956) was A7 + F6V. Tables from Pecaut & Mamajek (2013) estimate an effective temperature for the primary star, where $T_{\rm eff1}$= 7760 (125) K and log g = 4.282 (1) (cgs); the errors correspond to differences over one-half spectral subclass. An interpolation program (Nelson 2013) provided the van Hamme (1993) limb darkening values using the logarithmic (LD=2) law and are listed in Table 4. Values for the gravity darkening exponent g = 1.00 and albedo A = 1.0, appropriate for radiative stars (Lucy 1967; Ruciński 1969), respec-

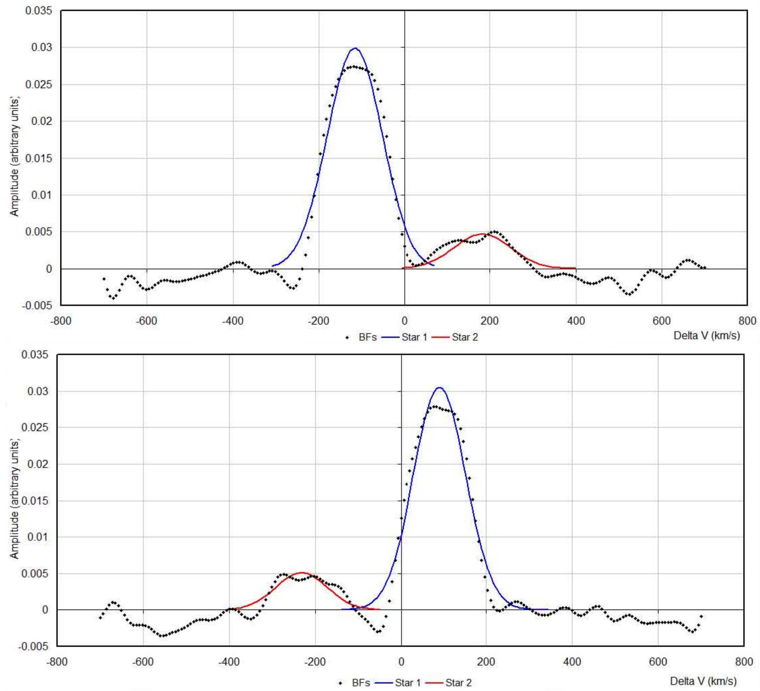

Fig. 3. Top: Broadening function for V1241 Tau at phase 0.248 and the fitted Gaussian profiles. The standard spectrum is 15-12961 (HD 187691) and the program spectrum, 15-13082. Bottom: Broadening function for V1241 Tau at phase 0.758 and the fitted Gaussian profiles. The standard spectrum is 15-12961 (HD 187691) and the program spectrum, 15-13018. The colour figure can be viewed online.

TABLE 3

V1241 TAU, COMPARISON AND CHECK STARS FOR APERTURE PHOTOMETRY

Object	GSC	RA (J2000)	Dec (J2000)	V-mag	$(B-V)$
V1241 Tau	4709-1181	03:24:23.25	-00:42:14.93	9.43	0.61 (35)
Comp.	4709-1022	03:24:28.57	-00:37:13.92	10.16 (4)	1.14 (4)
Check	4709-1298	03:24:42.57	-00:45:58.62	11.47 (1)	1.23 (2)

TABLE 4

LIMB DARKENING VALUES FROM VAN HAMME (1993)*

Band	x_1	x_2	y_1	y_2
B	0.829	0.843	0.851	0.035
V	0.719	0.795	0.791	0.152
I_c	0.506	0.656	0.639	0.205
Bol	0.673	0.635	0.647	0.174

*Based on spectral type A7, K0 for stars 1 and 2 respectively.

tively, were chosen. Model fit optimization was accomplished by differential corrections.

Final models using the TESS (2018) and land-based (2017-2019) light curves produced very similar effective temperatures for the secondary, where $T_{\rm eff2}$=5087 K and 5073 K, respectively. These values are much cooler than what would be expected from its putative F6V classification (6340 K) and correspond more closely to spectral class K0. In this case, the secondary limb darkening coefficients x_2, y_2 provided in Table 4 were determined using the mean value (5080 K).

Based on the shape of the BVI$_{\rm c}$ light curves (Figure 4), mode 5 (classical Algol) was selected but with the understanding that other modes such as mode 2-detached, mode 4-reverse Algol, etc. would need to be checked. Initially, convergence by the method of multiple subsets was reached. The subsets were: (a, i, Ω_1, $L1$), (i, q), (T_2, Ω_1), and (a, V_γ, ϕ). However, despite multiple iterations using different starting points, the resulting fits were rather poor.

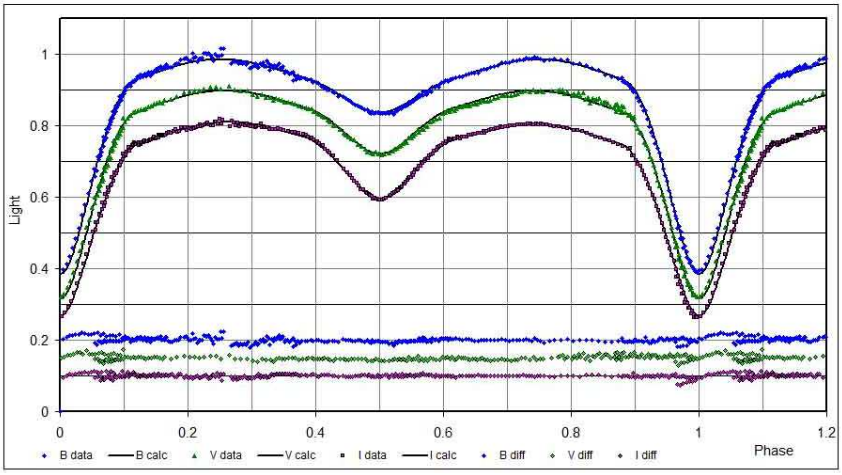

Fig. 4. Peak normalized V1241 Tau light curves from DBO with the WD results, separated by fixed offsets (0.1 light curve units). Plotted are, top to bottom: B, V, I_c. At the bottom of the figure, the model fit residuals are provided in the same order as the light curves. The colour figure can be viewed online.

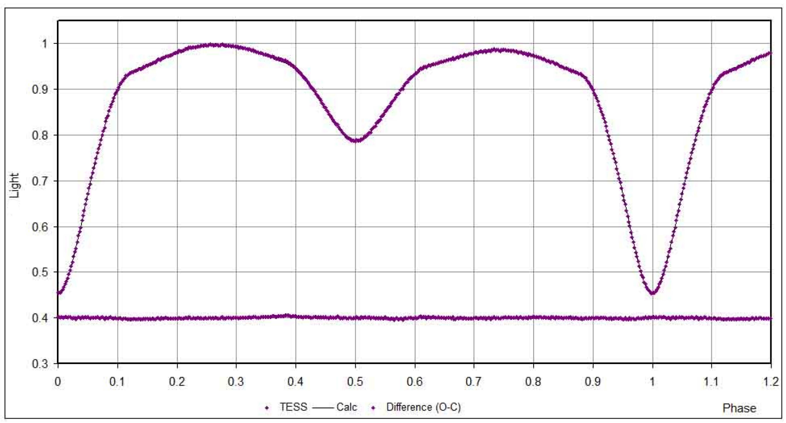

Fig. 5. Peak normalized V1241 Tau light curve and the WD results from the TESS Mission (2018). At the bottom of the figure, the residual differences between the observed and simulated light curve fits are plotted with a fixed offset (0.4). The colour figure can be viewed online.

As a consequence we turned to the light curve data taken by the TESS satellite in 2018. Parameter estimates for the best-fit TESS model are listed in Table 5 while the light curve (data and computed) are presented in Figure 5. Next, we returned to the DBO data and used the best-fit TESS parameters to get started. A reasonable fit quickly ensued with only minor adjustments required to reach an acceptable solution (Figure 4). The DBO parameters, listed in Table 5, differ only slightly from those obtained from the TESS data. The spot parameters (cool spot on the secondary star), which might be expected to change in the time interval between the two data sets, do so, but only by a small amount. Although secular analysis of minimum times (Yang et al. 2012) suggested the presence of a third gravitationally bound stellar object ($P{\approx}47.4$ y), it was not necessary to invoke a third light correction (l_3) to produce a satisfactory Roche-lobe model fit. Furthermore, no evidence for oscillation of either star in this binary system was found, thereby confirming that V1241 Tau should not be classified as an oEA system (Mkrtichian et al. 2003).

The radial velocity observations with the best double-sine curve model fit are plotted in Figure 6. This analysis yielded values for K_1 (101.6 ± 1.8 km$\cdot$s^{-1}), K_2 (205.5 ± 4.0 km$\cdot$s^{-1}) and V_γ (17.4 ± 1.8 km$\cdot$s^{-1}). When modeled without any light curve data, the spectroscopic mass ratio ($q_{\rm sp}=M_2/M_1$) was determined to be 0.495 ± 0.012.

TABLE 5

WILSON-DEVINNEY PARAMETERS FOR THE BEST-FIT SOLUTION FROM V1241 TAU LIGHT CURVES

WD Quantity[a]	TESS	DBO
$T_{\rm eff1}$ (K)[b]	7760	7760
$T_{\rm eff2}$ (K)	5087 (3)	5073 (8)
q (m$_2$/m$_1$)	0.543 (2)	0.544 (1)
Ω_1	3.465 (5)	3.470 (8)
i°	80.18 (4)	79.69 (3)
a (R$_\odot$)	5.30 (3)	5.39 (5)
V_γ (km·s^{-1})	18.7 (7)	18.7 (2)
$A_{\rm P} = T_{\rm S}/T_\star$[c]	0.832 (1)	0.855 (5)
$\Theta_{\rm P}$(spot co-latitude)[c]	86 (1)	92 (4)
$\phi_{\rm P}$ (spot longitude)[c]	288 (1)	310 (2)
r$_{\rm P}$ (angular radius)[c]	19.0 (1)	14.5 (5)
$L_1/(L_1+L_2)_{\rm B}$[d]	...	0.937 (1)
$L_1/(L_1+L_2)_{\rm V}$	...	0.888 (1)
$L_1/(L_1+L_2)_{\rm TESS,\ I_c}$	0.817 (1)	0.811 (1)
r_1 (pole)	0.3389 (6)	0.3390 (9)
r_1 (point)	0.3708 (10)	0.3700 (13)
r_1 (side)	0.3499 (7)	0.3500 (10)
r_1 (back)	0.3611 (8)	0.3610 (12)
r_2 (pole)	0.3064 (3)	0.3060 (20)
r_2 (side)	0.3199 (3)	0.3200 (20)
r_2 (back)	0.3523 (3)	0.3520 (20)

[a]All uncertainty estimates for Teff$_2$, q, $\Omega_{1,2}$, i, $r_{1,2}$, and L_1 from $WDwint56a$ (Nelson 2013).
[b]Fixed with no error during DC.
[c]Spot parameters in degrees ($\Theta_{\rm P}$, $\phi_{\rm P}$ and $r_{\rm P}$); A$_{\rm P}$ equals the spot temperature ($T_{\rm S}$) divided by star temperature, T_*.
[d]L_1 and L_2 refer to scaled luminosities of the primary and secondary stars, respectively.

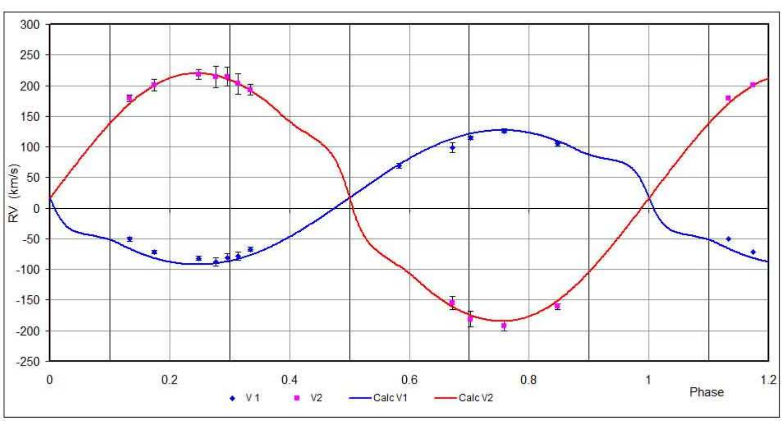

Fig. 6. V1241 Tau radial velocities and WD solution. As the computed curves from the DBO and TESS data sets were visually identical, only one RV plot is presented. The colour figure can be viewed online.

Simultaneous WD2003 analysis using the TESS data (regarded to have the least uncertainty) yielded M_1=1.91(8) M$_\odot$, M_2=1.04(4) M$_\odot$, R_1=1.86(1) R$_\odot$, R_2=1.73(1) R$_\odot$, $q_{\rm WD}$=0.54(3), L_1=10.7(8) L$_\odot$, and L_2=1.7(2) L$_\odot$. Note that the mass ratio in Table 5 derived from combined (RV+LC) fitting differs

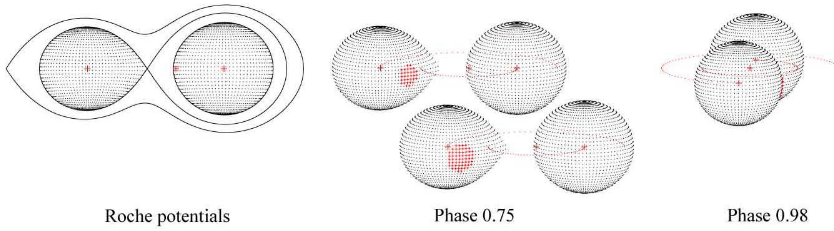

Fig. 7. Roche surface potentials and spatial representations of V1241 Tau from Binary Maker 3 showing a cool spot on the secondary star. At phase 0.75, the upper middle figure is from the DBO data (2017–2019), while the lower is from the TESS Mission (2018). The spatial orientation at phase 0.98 clearly shows the V1241 Tau is partially eclipsing. The colour figure can be viewed online.

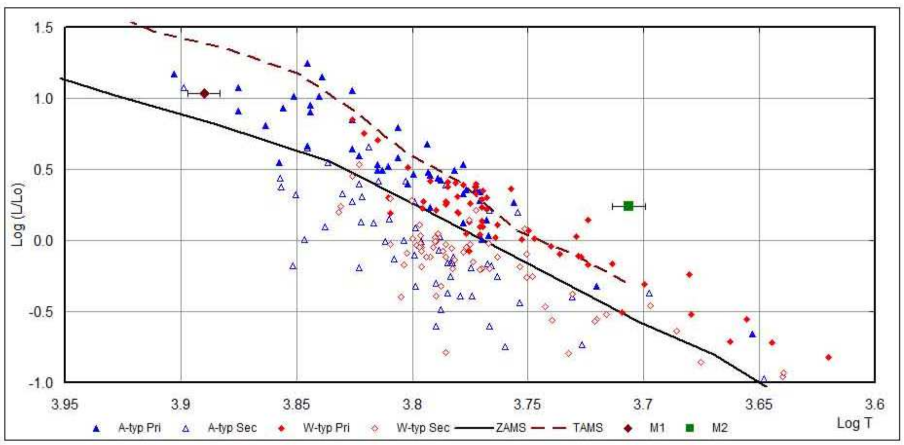

Fig. 8. log $L/\mathrm{L}_\odot$ vs log T plot for close binaries from Yakut and Eggleton (2005). The ZAMS (solid line) and the TAMS (dashed line) are from the evolutionary tracks of the Geneva Group (Schaller et al. 1992) when Z = 0.02 (solar-like). Results from the TESS satellite have been added: the large diamond (brown in the online version) is for the primary star while the large (green) square is for the secondary. The (half) width of each error bar is the standard deviation of the values for $T_{\mathrm{eff}1,2}$ and $\log L_{1,2}$ from each solution. The colour figure can be viewed online.

somewhat from the spectroscopic mass ratio directly calculated from the K_1/K_2 ratio. This is not unexpected; however, the latter value (0.543 ± 0.002) is considered more reliable since it is derived from all the data (Wilson 1990). In any case, WD parameter uncertainty from both light curve sources are quite comparable.

A word about error estimation is appropriate here (all error values in this paper are one sigma). For the errors in K_1 and K_2, the reader should consult Alton et al. (2020). For the individual RV data points in the present data set, each RV is the mean of values obtained from eight different standards; the error estimate is simply the standard deviation of the group. Actual errors from systematic effects are obviously larger but not directly calculable. That is why the sample standard deviation (i.e., sigma divided by root n) is not used as it would imply a greater precision than what is experienced. WD2003 parameter values with associated uncertainty following Roche-lobe modeling are listed in Table 5. These are statistical values known to be smaller than the total uncertainty because the latter contains systematic experimental errors not readily determined. Spatial representations of V1241 Tau rendered with Binary Maker 3 (Bradstreet 1993) are illustrated in Figure 7.

6. EVOLUTIONARY STATUS OF V1245 TAU

We can attempt to describe the evolutionary status of this variable using our estimates for luminosity and effective temperature. These values are plotted in the theoretical Hertzsprung-Russell diagram (HRD) from Yakut & Eggleton (2005) who evaluated 72 close binary systems for which reliable data existed. Types included were low-temperature overcontact binaries, near-contact binaries and detached close binaries. A reproduction of this log $L/\mathrm{L}_\odot$ vs. log T plot (Figure 8) includes zero-age main sequence

(ZAMS) values for selected stars from Cox (2000), and the terminal-age main sequence (TAMS) values from the evolutionary tracks of the Geneva Group (Schaller et al. 1992) when Z = 0.02 (solar). This analysis suggests that both stars have evolved, while the secondary might be past the TAMS. Nonetheless, one should regard plots of this type with much caution, as we do not know the metallicity plus there is a fairly large degree of uncertainty with the temperatures and luminosities for this system. The error bars hint at that uncertainty.

7. CONCLUSIONS

New radial velocity and light curve data for V1241 Tau, an Algol-type binary, have been simultaneously analysed with the Wilson-Devinney (WD2003) code. There were two distinct LC datasets: One was from the TESS space satellite and the other from a land-based (Desert Blooms) observatory. The RV data alone yielded results for K_1 (101.6 ± 1.8 km·s^{-1}), K_2 (205.5 ± 4.0 km·s^{-1}), RV$_\gamma$ (17.4 ± 1.8 km·s^{-1}), and $q_{\rm sp}$ (0.495 ± 0.012). Simultaneous analyses (RV+LC) using the TESS data resulted in the best estimates for M_1 (1.91 ± 0.08 M$_\odot$), M_2 (1.04 ± 0.04 M$_\odot$), R_1 (1.86 ± 0.01 R$_\odot$), R_2 (1.73 ± 0.01 R$_\odot$), $q_{\rm WD}$ (0.54 ± 0.03), L_1 (10.7 ± 0.8 L$_\odot$), and L_2 (1.7 ± 0.02 L$_\odot$). Simultaneous analysis with the DBO data yielded similar parameter values but often with greater uncertainties. Evolutionary analysis using an HRD model from Yakut and Eggleton (2005) suggested that the primary star in V1241 Tau is somewhat evolved past the zero age main sequence (ZAMS) while the secondary has evolved past the terminal age main sequence (TAMS). This is typical behaviour for many Algol-type binaries.

This research has made use of the SIMBAD database operated at Centre de Données astronomiques de Strasbourg, France. This work also presents results from the European Space Agency (ESA) space mission Gaia. Gaia data are being processed by the Gaia Data Processing and Analysis Consortium (DPAC). Funding for the DPAC is provided by national institutions, in particular those participating in the Gaia MultiLateral Agreement (MLA). The Gaia mission website is https://www.cosmos.esa.int/gaia, while the Gaia archive website is https://archives.esac.esa.int/gaia. This paper also makes use of TESS data obtained from the Mikulski Archive for Space Telescopes (MAST) at the Space Telescope Science Institute. STScI is operated by the Association of Universities for Research in Astronomy, Inc., under NASA contract NAS5-26555. Support to MAST for these data is provided by the NASA Office of Space Science via grant NAG5-7584 and by other grants and contracts. It is a pleasure to thank the staff members at the DAO (David Bohlender, Dmitry Monin) for their usual splendid help and assistance. Thanks are also due to Environment Canada for the website satellite images (https://weather.gc.ca/canada_e.html) that were essential in predicting clear times for observing runs in this cloudy locale, and to Attilla Danko and Allan Rahill of the CMC for their Clear Sky Chart (http://cleardarksky.com/). The diligence and dedication shown by all associated with these organizations is very much appreciated.

REFERENCES

Alton, K. B., Nelson, R. H., & Stępień, K. 2020, JApA, 41, 26, https://doi.org/10.1007/s12036-020-09641-y

Andrych, K. D. & Andronov, I. L. 2019, OEJV, 197, 65, https://doi.org/10.48550/arXiv.1812.06949

Andrych, K. D., Andronov, I. L., & Chinarova, L. L. 2020, JPhSt, 24, 1902, https://doi.org/10.30970/jps.24.1902

Arentoft, T., Lampens, P., van Cauteren, P., et al. 2004, A&A, 418, 249, https://doi.org/10.1051/0004-6361:20034543

Bradstreet, D. H. 1993, IAUS 151, Light Curve Modelling of Eclipsing Binary Stars, 151

Caldwell, D. A. 2020, RNAAS, 4, 201, https://doi.org/10.3847/2515-5172/abc9b3

Cox, A. N. 2000, Allen's Astrophysical Quantities, (New York, NY: Springer-Verlag)

Eastman, J., Siverd, R., & Guadi, B. S. 2010, PASP, 122, 935, https://doi.org/10.1086/655938

Gaia Collaboration et al. 2021, A&A, 649, 1, https://doi.org/10.1051/0004-6361/202039657

Gaposchkin, S. 1953, AnHar, 113, 67

Giuricin, G. & Mardirossian, F. 1981, A&AS, 45, 85

Henden, A. A., Welch, D. L., Terrell, D., & Levine, S. E. 2009, AAS, 41, 669

Hoffmeister, C. 1934, AN, 251, 19, https://doi.org/10.1002/asna.19342510203

Jensch, A. 1934, AN, 251, 327, https://doi.org/10.1002/asna.19342512104

Kallrath, J., Milone, E. F., Terrell, D., & Young, A. T. 1998, ApJ, 508, 308, https://doi.org/10.1086/306375

Karampotsiou, E., Gazeas, K., Petropouou, M., & Tzouganatos, L. 2016, IBVS, 6158, 1

Kazarovets, E. V., Samus, N. N., Durlevich, O. V., Kireeva. N. N., & Pastukhova, E. N. 2006, IBVS, 5721, 1

Kholopov, P. 1982, New catalogue of stars suspected of variability containing data on 14810 variable stars which have not received definite nomenclature until 1980 (Moskva: Nauka)

Kurucz, R. L. 1993, IAUCB 21, Light Curve Modeling of Eclipsing Binary Stars, 93, (New York, NY: Springer)
Lehký, M., Hoňková, K., Šmelcer, L., et al. 2021, OEJV, 211, 11, https://doi.org/10.5817/OEJV2021-0211
Lucy, L. B. 1967, ZA, 65, 89
Mkrtichian, D. E., Nazarenko, V., Gamarova, A. Y., et al. 2003, ASPC 292, Interplay of Periodic, Cyclic and Stochastic Variability in Selected Areas of the H-R Diagram, ed. C. Sterken (San Francisco, CA: ASP), 113
Nagai, K. 2014, VSOLJ Variable Star Bulletin, 56, 1
__________. 2015, VSOLJ Variable Star Bulletin, 59, 6
__________. 2021, VSOLJ Variable Star Bulletin, 69, 12
Nelson, R. H. 2010, Spectroscopy for Eclipsing Binary in The Alt-Az Initiative, Telescope Mirror & Instrument Developments, ed. R. M. Genet, J. M. Johnson, & V. Wallen (Santa Margarita, CA: Collins Foundation Press)
__________. 2013, Software, http://binaries.boulder.swri.edu/binaries/
__________. 2016, IBVS, 6164, 1
__________. 2017, IBVS, 6195, 1
__________. 2018, IBVS, 6234, 1
__________. 2020a, JAVSO, 48, 169
__________. 2020b, NewA, 77, 101362, https://doi.org/10.1016/j.newast.2020.101362
__________. 2022, RMxAA, 58, 223, https://doi.org/10.22201/ia.01851101p.2022.58.02.05
Pecaut, M. J. & Mamajek, E. E. 2013, ApJ, 208, 9, https://doi.org/10.1088/0067-0049/208/1/9
Pickering, E. C. 1908, AN, 178, 157, https://doi.org/10.1002/asna.19081781003
Pojmanski, G. 2003, AcA, 53, 341
Ricker, G. R., Winn, J. N., Vanderspek, R., et al. 2015, JATIS, 1, 014003
Roman, N. G. 1956, ApJ, 123, 246, https://doi.org/10.1086/146155
Russo, G. & Milano, L. 1983, A&AS, 52, 31
Ruciński, S. M. 1969, AcA, 19, 245
__________. 1992, AJ, 104, 1968, https://doi.org/10.1086/116372
__________. 2004, IAUS 215, Stellar Rotation, ed. A. Maeder & P. Eenens (San Francisco, CA: IAUS, 17)
Samolyk, G. 2020, JAVSO, 48, 87
Samus N. N., Kazarovets E. V., Durlevich O. V., Kireeva, N. N., & Pastukhova, E. N. 2017, ARep, 61, 80, https://doi.org/10.1134/S1063772917010085
Sarma, M. B. K. & Abhyankar, H. D. 1979, Ap&SS, 65, 443, https://doi.org/10.1007/BF00648509
Schaller, G., Schaerer, D., Meynet, G., & Maeder, A. 1992, A&AS, 96, 269
Stefanik, R. P., Latham, D. W., & Torres, G. 1999, ASPC 185, Precise Stellar Radial Velocities, ed. J. B. Hearnshaw & C. D. Scarfe, 354
Srivastava, J. B. & Kandpal, C. D. 1986, Ap&SS, 121, 301, https://doi.org/10.1007/BF00653701
Terrell, D. 2022, Galaxies, 10, 8, https://doi.org/10.3390/galaxies10010008
Terrell, D. & Wilson, R. W. 2005, Ap&SS, 296, 221, https://doi.org/10.1007/s10509-005-4449-4
van Hamme, W. 1993, AJ, 106, 2096, https://doi.org/10.1086/116788
Wilson, R. E. & Devinney, E. J. 1971, ApJ., 166, 605, https://doi.org/10.1086/150986
Wilson, R. E. 1990, ApJ, 356, 613, https://doi.org/10.1086/168867
Yakut, K. & Eggleton, P. P. 2005, ApJ, 629, 1055
Yang, Y.-G., Zhang, X.-B., Li, H.-L., & Dai, H. F. 2012, AJ., 144, 136, https://doi.org/10.1088/0004-6256/144/5/136

Kevin B. Alton: Desert Blooms Observatory, 70 Summit Ave., Cedar Knolls, AZ, USA (mail@underoakobservatory.com).
M. Kendurkar: Dominion Astrophysical Observatory, 5071 W Saanich Rd, Victoria, BC V9E 2E7, Canada.
R. H. Nelson: Mountain Ash Observatory, 1393 Garvin Street, Prince George, BC, Canada, V2M 3Z1.